Transition state for the NSD2-catalyzed methylation of histone H3 lysine 36

Myles B. Poulin[a], Jessica L. Schneck[b], Rosalie E. Matico[b], Patrick J. McDevitt[b], Michael J. Huddleston[b], Wangfang Hou[b], Neil W. Johnson[c], Sara H. Thrall[b], Thomas D. Meek[b,1], and Vern L. Schramm[a,2]

[a]Department of Biochemistry, Albert Einstein College of Medicine of Yeshiva University, Bronx, NY 10461; [b]Biological Sciences, Platform Technology and Science, GlaxoSmithKline, Collegeville, PA 19426; and [c]Cancer Epigenetics Discovery Performance Unit, GlaxoSmithKline, Collegeville, PA 19426

Nuclear receptor SET domain containing protein 2 (NSD2) catalyzes the methylation of histone H3 lysine 36 (H3K36). It is a determinant in Wolf–Hirschhorn syndrome and is overexpressed in human multiple myeloma. Despite the relevance of NSD2 to cancer, there are no potent, selective inhibitors of this enzyme reported. Here, a combination of kinetic isotope effect measurements and quantum chemical modeling was used to provide subangstrom details of the transition state structure for NSD2 enzymatic activity. Kinetic isotope effects were measured for the methylation of isolated HeLa cell nucleosomes by NSD2. NSD2 preferentially catalyzes the dimethylation of H3K36 along with a reduced preference for H3K36 monomethylation. Primary Me-^{14}C and ^{36}S and secondary Me-^{3}H$_3$, Me-^{2}H$_3$, 5′-^{14}C, and 5′-^{3}H$_2$ kinetic isotope effects were measured for the methylation of H3K36 using specifically labeled S-adenosyl-L-methionine. The intrinsic kinetic isotope effects were used as boundary constraints for quantum mechanical calculations for the NSD2 transition state. The experimental and calculated kinetic isotope effects are consistent with an S_N2 chemical mechanism with methyl transfer as the first irreversible chemical step in the reaction mechanism. The transition state is a late, asymmetric nucleophilic displacement with bond separation from the leaving group at (2.53 Å) and bond making to the attacking nucleophile (2.10 Å) advanced at the transition state. The transition state structure can be represented in a molecular electrostatic potential map to guide the design of inhibitors that mimic the transition state geometry and charge.

enzyme mechanism | transition state structure | histone methylation | kinetic isotope effects

Histone lysine methylation is an essential posttranslational modification for transcriptional regulation, DNA damage response, and chromatin regulation (1, 2). Methyl groups (Me, CH$_3$) are installed on lysine residues by protein lysine methyltransferase enzymes (PKMTs), the majority of which, in humans, contain a catalytic SET domain (3). The conserved SET domain catalyzes the transfer of between one to three CH$_3$ from S-adenosyl-L-methionine (SAM) onto the ε-amino group of lysine residues (Fig. 1) producing monomethyl, dimethyl, or trimethyl lysine derivatives (KMe1, KMe2, and KMe3, respectively) (3), in a reaction that involves first deprotonation of the lysine, and finally transfer of the methyl group (4, 5).

Histone lysine Me marks can signal either transcriptional activation or repression depending on which lysine residue is methylated and the number of transferred Me groups (2). For example histone H3 lysine 27 trimethylation is a signal for transcriptional repression (6), where histone H3 lysine 4 and histone H3 lysine 36 Me marks are found in actively transcribed loci (7). As a result, misregulation of PKMT expression is often associated with cancer development and other disease states (8). Deletion of the gene encoding the histone H3K36 dimethyltransferase enzyme nuclear receptor binding SET domain protein 2 (NSD2) (also known as WHSC1 or MMSET), specifically, is present in the developmental disorder Wolf–Hirschhorn syndrome (9). By contrast, NSD2 overexpression, as a result of a

t(4;14) chromosomal translocation (10), is manifest in 15% of multiple myeloma cases and has been identified in other cancers (11–13). NSD2 catalyzes the monomethylation and dimethylation of histone H3K36 in vivo (11), although other CH$_3$-transfer specificities have also been reported in studies using histone protein or histone tail peptide as substrate analogs (14–16). Studies using isolated or recombinant nucleosome as physiologically relevant substrates detected H3K36Me1 and H3K36Me2 as the exclusive products. Thus, the nature of the substrate can influence NSD2 specificity (11, 17). Substrate specificity is also influenced by the presence of a C-terminal basic post-SET extension found in NSD family methyltransferases. NSD2 mutants lacking this basic post-SET extension are unable to recognize nucleosome as substrate (18). The H3K36Me2 marks introduced by NSD2 are normally concentrated in the 5′ end of actively transcribed genes (7), and overexpression results in global increases in H3K36Me2 throughout gene bodies, resulting in aberrant transcription of multiple oncogenes (11). Histone methylation is a reversible posttranslational modification, thus, inhibiting the catalytic activity of NSD2 is an attractive strategy for the treatment of multiple myeloma and other cancers.

Designing analogs that mimic the geometry and charge distribution of the transition state (TS) of enzyme-catalyzed reactions is a powerful approach for enzyme inhibition (19, 20); however, this requires a detailed model of the enzyme TS. TS models for a number of PKMT enzymes, including human SET8 (21), and SET7/9 (4, 22), based on quantum mechanical (QM)/molecular mechanical (MM) calculation of the enzyme

---

Significance

Epigenetic control by methylation of histones is essential in development. Loss of regulation of methylation pathways is involved in developmental disorders and oncogenesis. Despite interest in NSD2, there have been no selective inhibitors reported. Analogs designed to mimic the NSD2 transition state structure are potential enzyme inhibitors. A combination of experimental kinetic isotope effects and quantum chemistry was used to define the subangstrom details of reaction chemistry at the transition state of NSD2. Electrostatic potential maps of reactants and transition states provide a high-resolution map of reaction chemistry and a blueprint for design of transition state analogs for this mechanism of epigenetic regulation.
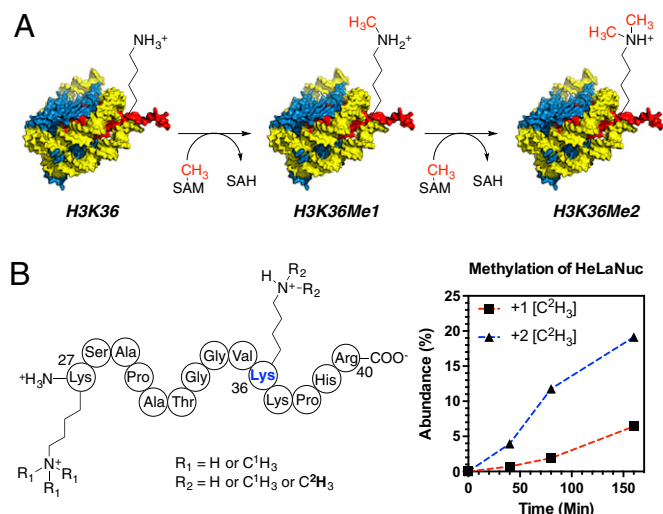

BIOCHEMISTRY

Fig. 1. NSD2-catalyzed methylation of histone H3 lysine 36 (H3K36). (*A*) The general reaction catalyzed by NSD2 showing both monomethylation and dimethylation of H3K36. (*B*) Product distribution for methylation of HeLaNuc with [Me-^{2}H$_3$]SAM. Products are shown for the histone H3 (K27–R40) peptide resulting from Arg-C digestion. NSD2 displays a preference for dimethylation H3K36.

chemistry, show substantial variability in the predicted TS geometry of PKMT. However, these models have not been verified experimentally. Detailed information about TS structure can be obtained from the measurement of kinetic isotope effects (KIEs) (23), which result from changes in the bond vibrational environment for atoms of the reactants free in solution and at the TS (23). The measurement of multiple KIEs combined with quantum chemical calculations allow for interrogation of TS structure (19, 20, 24). Here, we apply this approach for the NSD2-catalyzed methylation of histone H3K36. Multiple experimental KIEs for the methylation of HeLa cell nucleosome (HeLaNuc) H3K36 by the SET domain of NSD2 were measured, and the KIEs were used to evaluate quantum chemical models of the CH$_3$-transfer TS.

Results and Discussion

NSD2 Dimethylates Histone H3 at Lysine 36 of HeLaNucs. The substrate and product specificity of NSD2 is dependent on both the nature of the substrate and the NSD2 construct used (17, 18). We analyzed the product distribution using extracted HeLaNuc as a mimic of the native substrate and a NSD2 construct containing the C-terminal SET domain and basic post-SET extensions (residues 980–1365). HeLaNuc contain a heterogeneous mixture of preexisting methyl marks (25). The installation of new methyl marks was tracked using [Me-^{2}H$_3$]SAM and the products monitored by liquid chromatography–mass spectrometry (LC-MS) after protease digestion (Fig. 1). Under these conditions, we observed only monomethylation and dimethylation of histone H3K36 regardless of the preexisting methylation state in the parent nucleosome, consistent with previous reports of wild-type NSD2 specificity (Fig. S1) (11, 17). We also observed no trimethylated H3K36, consistent with reports that SETD2 is the only known human H3 K36 trimethyltransferase (26). These results indicate the specificity of our NSD2 construct was not altered by truncation of the N-terminal domains. These results indicate that the N-terminal domains of NSD2 do not directly affect the enzyme chemistry and, likely, do not affect the TS structure.

Measurement of Intrinsic KIEs and Forward Commitment. KIEs for methylation of HeLaNuc histone H3K36 by NSD2 were measured using a competitive radiolabel approach. Under these

conditions, the observed KIEs on V_{max}/K_M (V/K) include contributions from all isotopically sensitive steps up to and including the first irreversible reaction, which for PKMT is generally accepted to be CH$_3$-transfer (5). Thus, any events preceding CH$_3$-transfer, including substrate binding and lysine deprotonation, can lead to an observed forward commitment (C_f), which would lower the magnitude of measured KIEs. C_f is a measure of the distribution of enzyme-bound substrate that proceeds to form product rather than equilibrate with free substrate. Using the isotope-trapping method (27), we measured a C_f of 0.087 ± 0.003 for the reaction of SAM with NSD2$_{SET}$ (Fig. 2*A*). This C_f is relatively low, indicating that events preceding CH$_3$-transfer are not significantly rate limiting, and Eq. **1** can be used to obtain intrinsic KIEs (k) required for TS analysis, where (V/K) is the observed KIE:

$$(V/K) = (k + C_f)/(1 + C_f). \quad [1]$$

Isotopically-labeled SAM for KIE measurements were prepared enzymatically from appropriately labeled ATP or methionine precursors (Table S1). KIEs measured for the atomic positions surrounding the methyl-transfer reaction coordinate are summarized in Table S2 and Fig. 2*B*. Each KIE was determined under competitive conditions using a "heavy" substrate, bearing a ^{3}H or ^{14}C at the position of interest, and a "light" substrate with a remote radiolabel reporting on the corresponding light isotope at the position of interest. For Me-^{2}H$_3$ and ^{36}S, the heavy substrates also contained a remote 1′-^{3}H or 8-^{14}C label. KIEs were determined from the change of isotope ratio of the unreacted SAM after 15–45% had been consumed. Correcting for C_f gave an intrinsic primary Me-^{14}C KIE of 1.113 ± 0.006, primary ^{36}S KIE of 1.018 ± 0.008, and secondary Me-^{3}H$_3$, 5′-^{14}C, and 5′-^{3}H$_2$ KIEs of 0.77 ± 0.03, 1.00 ± 0.01, and 1.05 ± 0.01, respectively.
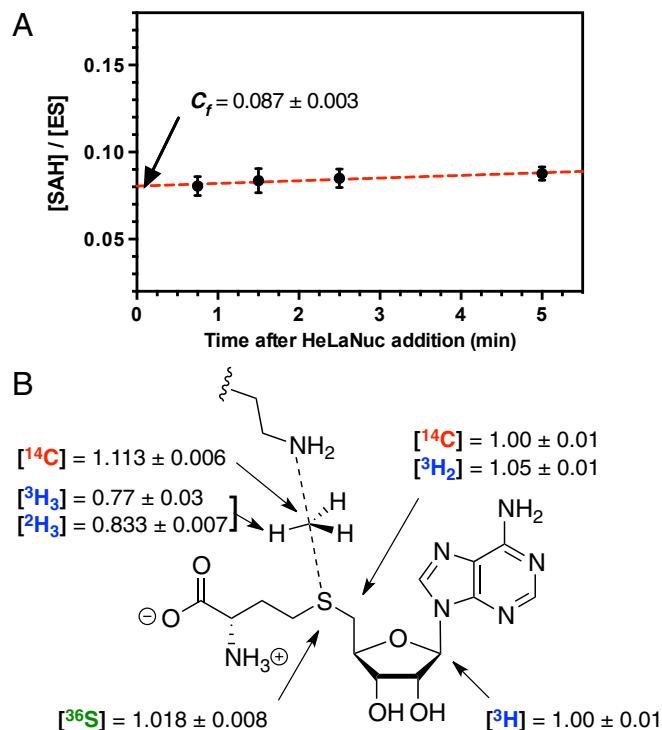

Fig. 2. Determination of intrinsic KIEs and correction for forward commitment factor (C_f). (*A*) Measurement of C_f by isotope trapping for the methylation of HeLaNuc H3K36 by NSD2. (*B*) Intrinsic KIE values by atom position after correction for C_f. Errors are reported as the SD of at least six replicates from two independent experiments.

A large primary ^{14}C KIE is consistent with an S_N2 mechanism where the CH_3-transfer is largely rate limiting. The magnitude of the primary KIE of the transferring methyl group for S_N2 reaction mechanisms is proportional to the symmetry of the TS structure, with the largest isotope effects expected when bond order to the nucleophile and leaving group are equal (28). A large inverse α-secondary ^{3}H KIE for the methyl group hydrogen of 0.77 ± 0.03 suggests the hydrogen vibrational modes are constrained at the TS relative to the ground state. To confirm the magnitude of this isotope effect, we also measured the α-secondary Me-[2]H$_3$ KIE. The intrinsic Me-[2]H$_3$ KIE of 0.833 ± 0.007 is in good agreement with the Me-[3]H$_3$ isotope effect given the difference in the reduced mass of each isotope (29). Such large inverse α-secondary KIEs have previously been observed for the methylation of catechol substrates by catechol O-methyltransferase (COMT) (30, 31). In that case, the large inverse KIE was attributed to compression of the methyl donor–acceptor distance at the TS (30). However, QM/MM calculations suggest that such compression is not required to explain the observed inverse KIEs (32, 33).

Computational Models of the NSD2 TS. The TS structure for methylation of H3K36 by NSD2 was modeled using the intrinsic KIEs as constraints. The reactant-state input for TS analysis was derived from the conformation of SAM in the crystal structure of NSD1 [Protein Data Bank (PDB) ID code 3OOI] (34), as no structure of NSD2 was available. The catalytic SET domain of NSD1 and NSD2 are highly homologous containing 79% sequence identity. To model the lysine position, the SET domain of NSD1 was overlaid with those of SET7/9, SET8, and PIM5 bound to their corresponding peptide substrates (Fig. 3A and Fig. S2) (35–37). The average lysine geometry was used to generate a simplified TS model (**TS1** in Fig. 3B).

The TS geometry for NSD2 can be described by a combination of the C–N and C–S distances, $d1$ and $d2$, shown in Fig. 3B. A series of TS structures with fixed $d1$ and $d2$ distances were calculated at the m062x/6-31G* level of theory, as implemented in

Gaussian 09 (38). No other constraints on the TS geometry or the S–C–N bond angle were imposed. Theoretical isotope effects for each geometry were predicted from the scaled vibrational frequencies using the program ISOEFF98 (Fig. 3C and Fig. S3) (39). Because NSD2 catalyzes both the monomethylation and dimethylation of H3K36, the observed KIEs could arise from the TS for either the first or second methylation reaction or a combination of the two. The same calculations were performed using a TS model for the second methylation reaction (Fig. S4). TS models for both the first and second methylation reaction catalyzed by NSD2 had highly similar predicted KIEs for all geometries tested, so for the sake of simplicity we will focus our discussion on the TS for the first methylation. In general, the predicted Me-^{14}C KIEs were larger (>1.12) for TS geometries with more symmetrical bond order to both the sulfur leaving group and nitrogen nucleophile, with a later, asymmetric TS matching the observed KIE of 1.113 (Fig. 3C). A number of TS geometries with compressed donor–acceptor distances predict inverse Me-[3]H$_3$ KIEs but gave poor agreement with the Me-^{14}C KIE. Instead, the predicted Me-[3]H$_3$ KIEs matched most optimally to TS geometries with greater bond order to the lysine nitrogen. Predicted [36]S KIEs are also consistent for a product-like TS geometry with substantial loss of bond order to the transferring CH_3 group at the TS. The closest match to all intrinsic KIEs was observed with $d1$ and $d2$ fixed at 1.8 and 2.6 Å, respectively, corresponding to a late product-like TS geometry; however, no TS geometry was able to reproduce the observed 5′-[3]H$_2$ KIE (Figs. S3 and S4). This KIE is highly dependent on the bound SAM geometry and was found to vary substantially as the result of rotation around the C5′–S bond in our simplified TS model (Fig. S5).

Previous work indicates QM tunneling can contribute to the magnitude of heavy-atom KIEs (40, 41). To assess the possibility that QM tunneling contributes to our observed Me-^{14}C KIE, we calculated predicted Me-^{14}C KIEs while including a correction for carbon tunneling. For our system, the magnitude of predicted KIEs including tunneling are larger than the intrinsic value for all TS geometries tested (Fig. S6), and, as a result, we did not include a tunneling correction in our final TS predictions.

Secondary hydrogen KIEs can also be influenced by geometric and electronic constraints imposed by the enzyme that are not reproduced using a simplified TS model. Previous QM/MM studies of COMT have shown that increasing the number of atoms included in the QM region impacts the predicted donor–acceptor geometry in the bound complex of COMT, SAM, and catechol (42). Thus, it is possible that including atoms from amino acids from NSD2 active-site residues in our QM calculation will influence the predicted KIEs. Here, we included the backbone carbonyls of R1138 and F1117 and side chain of Y1179, whose positions are conserved among SET domain containing PKMT, in our TS calculation (Fig. 4A) (43). The corresponding residues in SET7/9 are proposed to interact with the hydrogen atoms on the transferring methyl group (43, 44). Including these interactions in our model, we observed a match to all intrinsic KIEs with $d2$ fixed at 2.53 Å and $d1$ at 2.10 Å (**TS2** in Fig. 4A). The predicted Me-[3]H$_3$, Me-[2]H$_3$, and 5′-[3]H$_2$ KIEs were more inverse, or less normal, than those observed for a simplified TS model (**TS1**) with the same geometry, indicating the Me-H$_3$ and 5′-H$_2$ bond vibrational modes are more constrained in the presence of these active-site interactions. However, there is no evidence that the donor–acceptor distance is compressed in our TS model and the intrinsic KIEs for NSD2 are consistent with product-like TS models with a shorter bond to the nucleophilic nitrogen. The total donor–acceptor distance in this model is in good agreement with previous QM/MM calculations for related PKMTs that predict a range of possible TS geometries (21, 22, 45–48). Compared with the TS geometry calculated for other human PKMTs, the TS for NSD2 is more product-like, having a more dissociated C–S bond. This may allow for the design of NSD2-specific inhibitors that mimic a product-like TS geometry.
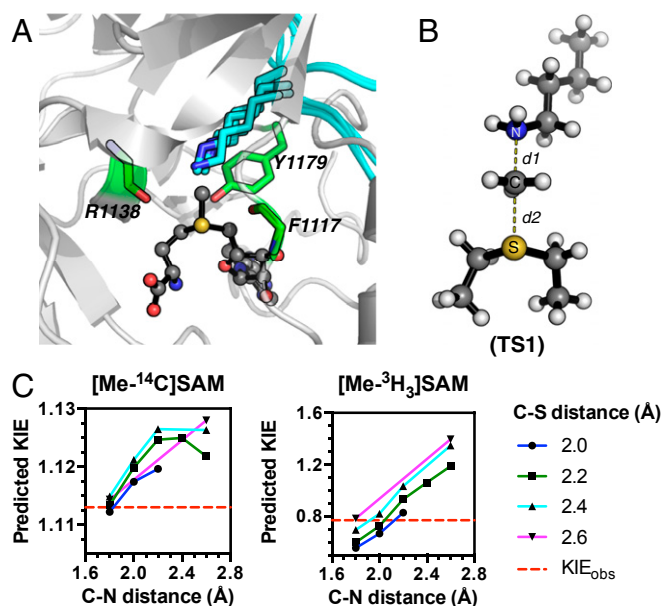
Fig. 3. Theoretical TS model for NSD2 methylation of H3K36. (A) A prediction of the lysine substrate geometry from the structure NSD1 overlaid with the with peptide substrates of SET7/9 (PDB ID codes 1XQH and 2F69) SET8 (PDB ID codes 3F9W and 3F9Y), and PIM5 (PDB ID code 1PEG) shown in cyan. (B) A simplified TS model for the NSD2 methyl-transfer reaction derived from the SAM and lysine geometry. (C) KIEs predicted for **TS1** at different fixed C–N and C–S distances.

Fig. 4. Geometry and electrostatic potential surface of the NSD2 TS structure. (*A*) TS structure for H3K36 methylation catalyzed by NSD2 with active-site amino acids F1117, M1140, and Y1179 (**TS2**). (*B*) Electrostatic potential surface map (EPSM) for **TS2** (red, partial negative; blue, partial positive). (*C*) A compa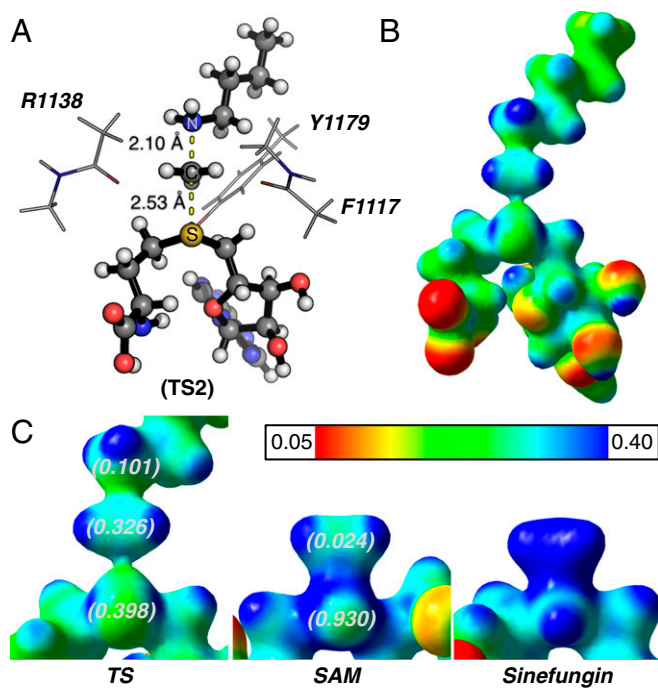rison of the EPSM for **TS2**, SAM, and methyltransferase inhibitor sinefungin. The NBO charge for the sulfur atom, CH_3 group (sum of carbon and hydrogen), and lysine NH_2 group are shown in parentheses for **TS2** and SAM.

TS Bond Order and Charge Distribution. The total bond order to both the leaving group and nucleophile in an S_N2 reaction can vary between 0, for an extremely loose TS, or greater than 1 for compressed TS geometry. By comparison, **TS2** has calculated bond orders of 0.382 and 0.482 for the C–S and C–N bonds, respectively. The sum of these bond orders is consistent with a loose donor–acceptor distance in the NSD2 TS structure. Fig. 4 highlights the electrostatic potential and natural bond orbital (NBO) charge distribution in **TS2** compared with that of SAM and the methyltransferase inhibitor sinefungin. A positive charge is predominantly localized on the sulfur atom of SAM in **GS2**, as indicated by the NBO charge of 0.930 for the sulfur atom compared with 0.024 for the Me group carbon and hydrogen. In **TS2**, the positive charge on sulfur is reduced to 0.398 with a corresponding increase for the Me group to 0.326, consistent with an S_N2 TS where the positive charge is distributed between the leaving group, transferring group, and nucleophile. The same distribution is observed for the electrostatic potential (Fig. 4*C*), where a positive electrostatic potential is localized on sulfur in SAM and distributed between the sulfur, methyl carbon, and lysine nitrogen in **TS2**. Analogs of sinefungin have been reported as selective inhibitors of SETD2 and proposed to mimic the TS of this enzyme (49). However, the electrostatic potential distribution for sinefungin appears to more closely mimic the charge localization of SAM than our **TS2** (Fig. 4*C*). It is likely that chemically stable analogs of the NSD2 TS will require that a positive charge be distributed between at least two atoms and located at least 2.5 Å from a neutral atom mimicking the leaving group sulfur. Work is currently underway to design such analogs.

Conclusions

NSD2 predominantly catalyzes the dimethylation of HeLaNuc on H3K36 in vitro, consistent with the activity of full-length NSD2

(11, 17). Using a combination of experimental KIE measurements and density functional theory calculations, we have determined a TS structure for the NSD2 SET domain-catalyzed methylation of histone H3K36. The intrinsic KIEs are consistent with an S_N2 reaction mechanism where methyl group transfer is significantly rate limiting. All of the intrinsic KIEs are consistent with a product-like TS geometry with a longer leaving group distance and shorter nucleophile distances of 2.53 and 2.10 Å, respectively. A comparison of electrostatic potential for the predicted TS structure and SAM GS indicate the positive charge on SAM is distributed between the leaving-group sulfur, the transferring methyl group, and the nitrogen nucleophile at the TS. This geometry and charge distribution can now guide future TS analog design for inhibitors of NSD2. Although a single TS structure for the NSD2-catalyzed monomethylation of H3K36 was sufficient to match the observed KIEs for the methylation of HeLaNuc, it is possible that the individual monomethylation and dimethylation reactions would produce different KIEs and TS structures. To address this, KIE studies using chemically defined nucleosome substrates that are either unmethylated or monomethylated at H3K36 are currently underway.

Materials and Methods

Materials. L-[Me-^{14}C]Methionine and L-[Me-^{3}H$_3$]methionine were purchased from PerkinElmer. D-[1-^{3}H]Ribose, D-[6-^{3}H$_2$]glucose, D-[6-^{14}C]glucose, and [8-^{14}C]adenine were purchased from American Radiolabeled Chemicals. L-[Me-^{2}H$_3$]Methionine was purchased from Cambridge Isotope Laboratories. Hexokinase pyruvate kinase, myokinase, phosphoriboisomerase, glucose-6-phosphate dehydrogenase, glutamic acid dehydrogenase, and 6-phospho-gluconic acid dehydrogenase were purchased from Sigma-Aldrich. Adenine phosphoribosyltransferase, phosphoribosyl-α-1-pyrophosphate synthetase, and ribokinase and SAM synthetase were prepared as previously described (50–52). HeLaNucs were extracted and purified as primarily mononucleosome and dinucleosome from cultured HeLa cells as previously described (53). Other chemicals and reagents were obtained from commercial sources and used without further purification. Human NSD2 SET domain (amino acid residues 980–1365) was expressed recombinantly and purified as described in *SI Materials and Methods*, and contained no bound SAM or S-adenosyl-L-homocysteine (SAH).

Methylation of HeLaNuc. NSD2 reaction mixtures containing 1 μM HeLaNuc, 100 nM NSD2, and 20 μM [Me-^{2}H$_3$]SAM in 50 mM Tris·HCl (pH 9.0) with 5 mM MgCl$_2$, 30 mM NaCl, 4 mM DTT, and 5% (mass/vol) glycerol were monitored by LC-MS to track newly installed methyl marks as described in *SI Materials and Methods*.

Synthesis of Isotope-Labeled SAM. 1′-^{3}H–, 5′-^{3}H$_2$–, and 5′-^{14}C–labeled ATPs were prepared as described previously (50). [8-^{14}C]ATP was synthesized enzymatically in an analogous manner using 8-^{14}C–labeled adenine (Fig. S1). [^{36}S]Methionine was prepared chemoenzymatically from ^{36}S-sulfur as previously described (54). 1′-^{3}H–, 5′-^{3}H$_2$–, 5′-^{14}C–, 8-^{14}C–, Me-^{3}H$_3$–, Me-^{14}C–, Me-^{2}H$_3$–, Me-^{2}H$_3$, 1′-^{3}H–, and ^{36}S, 8-^{14}C–labeled SAM were prepared using *Escherichia coli* SAMsyn from the corresponding labeled ATPs or methionines (Table S1) as described in *SI Materials and Methods*.

Measurement of KIEs and Forward Commitment. KIEs on *V/K* were measured using the competitive radiolabel approach (24, 50). SAM labeled at the atomic position of interest was mixed with an appropriate remote-labeled SAM bearing the light isotope at the position of interest shown in Table S2. KIEs were calculated from the change in isotope ratio in the remaining SAM substrate after 15–45% of the SAM substrate was consumed. Forward commitment (C_f) was measured using the isotope-trapping method (27). Detailed methods for the measurement of both KIEs and C_f are found in *SI Materials and Methods*.

Computational Methods. The TS for methyl transfer catalyzed by NSD2 was studied by density functional theory in m062X/6-31G* as implemented in Gaussian 09 (38). Starting coordinates for the TS were derived from an overlay of the crystal structures of NSD1 (PDB ID code 3OOI) (34), SET7/9 (PDB ID codes 2F69 and 1XQH) (35), SET8 (PDB ID codes 3F9Y and 3F9W) (Fig. 3 and Fig. S2) (36). Initial coordinates for **TS1** were located at a first-order saddle point and expanded to include *d1* of 1.8, 2.0, 2.4, and 2.6 Å and *d2* of 2.0, 2.2, 2.4, and 2.6 Å (Fig. S3). The same calculations were performed to

locate the TS for the second methylation reaction (Fig. S4). Coordinates for the low energy conformation of SAM in the PubChem 3D database was used for the SAM ground states (GS) (55). SAM GS conformations were calculated at the same level of theory including water as an implicit solvent. The GS were located at local minima and contained no imaginary frequencies. A final TS model, including 40 atoms from active-site residues derived from the crystal structure of NSD1 (3OOI) (34), was calculated at the m062X/6-31Gd* level of theory (TS2). These residues are conserved between NSD1 and NSD2. TS2 contains a single imaginary frequency corresponding to the methyl group transfer. KIEs for each TS structure were calculated from the scaled vibrational frequencies using ISOEFF98 with the appropriate GS structures. Coordinates for all TS models are available upon request.

NBO analysis was performed for TS2 and the SAM (Fig. 4) using the same level of theory. Electrostatic potential maps for TS2 and bound SAM were visualized in Gaussview 5.0 using potential and density cubes generated from the NBO calculations (isovalue, 0.04).

1. Kouzarides T (2007) Chromatin modifications and their function. *Cell* 128(4):693–705.
2. Jenuwein T, Allis CD (2001) Translating the histone code. *Science* 293(5532): 1074–1080.
3. Dillon SC, Zhang X, Trievel RC, Cheng X (2005) The SET-domain protein superfamily: Protein lysine methyltransferases. *Genome Biol* 6(8):227.
4. Zhang X, Bruice TC (2008) Enzymatic mechanism and product specificity of SET-domain protein lysine methyltransferases. *Proc Natl Acad Sci USA* 105(15):5728–5732.
5. Kipp DR, Quinn CM, Fortin PD (2013) Enzyme-dependent lysine deprotonation in EZH2 catalysis. *Biochemistry* 52(39):6866–6878.
6. Cao R, et al. (2002) Role of histone H3 lysine 27 methylation in Polycomb-group silencing. *Science* 298(5595):1039–1043.
7. Wozniak GG, Strahl BD (2014) Hitting the "mark": Interpreting lysine methylation in the context of active transcription. *Biochim Biophys Acta* 1839(12):1353–1361.
8. Schneider R, Bannister AJ, Kouzarides T (2002) Unsafe SETs: Histone lysine methyltransferases and cancer. *Trends Biochem Sci* 27(8):396–402.
9. Stec I, et al. (1998) WHSC1, a 90 kb SET domain-containing gene, expressed in early development and homologous to a *Drosophila* dysmorphy gene maps in the Wolf-Hirschhorn syndrome critical region and is fused to IgH in t(4;14) multiple myeloma. *Hum Mol Genet* 7(7):1071–1082.
10. Chesi M, et al. (1998) The t(4;14) translocation in myeloma dysregulates both FGFR3 and a novel gene, MMSET, resulting in IgH/MMSET hybrid transcripts. *Blood* 92(9): 3025–3034.
11. Kuo AJ, et al. (2011) NSD2 links dimethylation of histone H3 at lysine 36 to oncogenic programming. *Mol Cell* 44(4):609–620.
12. Morishita M, di Luccio E (2011) Cancers and the NSD family of histone lysine methyltransferases. *Biochim Biophys Acta* 1816(2):158–163.
13. Hudlebusch HR, et al. (2011) MMSET is highly expressed and associated with aggressiveness in neuroblastoma. *Cancer Res* 71(12):4226–4235.
14. Morishita M, Mevius D, di Luccio E (2014) In vitro histone lysine methylation by NSD1, NSD2/MMSET/WHSC1 and NSD3/WHSC1L. *BMC Struct Biol* 14(1):25.
15. Nimura K, et al. (2009) A histone H3 lysine 36 trimethyltransferase links Nkx2-5 to Wolf-Hirschhorn syndrome. *Nature* 460(7252):287–291.
16. Pei H, et al. (2011) MMSET regulates histone H4K20 methylation and 53BP1 accumulation at DNA damage sites. *Nature* 470(7332):124–128.
17. Li Y, et al. (2009) The target of the NSD family of histone lysine methyltransferases depends on the nature of the substrate. *J Biol Chem* 284(49):34283–34295.
18. Allali-Hassani A, et al. (2014) A basic post-SET extension of NSDs is essential for nucleosome binding in vitro. *J Biomol Screen* 19(6):928–935.
19. Schramm VL (2007) Enzymatic transition state theory and transition state analogue design. *J Biol Chem* 282(39):28297–28300.
20. Schramm VL (2011) Enzymatic transition states, transition-state analogs, dynamics, thermodynamics, and lifetimes. *Annu Rev Biochem* 80(80):703–732.
21. Zhang X, Bruice TC (2008) Product specificity and mechanism of protein lysine methyltransferases: Insights from the histone lysine methyltransferase SET8. *Biochemistry* 47(25):6671–6677.
22. Zhang X, Bruice TC (2007) Histone lysine methyltransferase SET7/9: Formation of a water channel precedes each methyl transfer. *Biochemistry* 46(51):14838–14844.
23. Cleland WW (1995) Isotope effects: Determination of enzyme transition state structure. *Methods Enzymol* 249:341–373.
24. Schramm VL (1999) Enzymatic transition-state analysis and transition-state analogs. *Methods Enzymol* 308:301–355.
25. Young NL, et al. (2009) High throughput characterization of combinatorial histone codes. *Mol Cell Proteomics* 8(10):2266–2284.
26. Wagner EJ, Carpenter PB (2012) Understanding the language of Lys36 methylation at histone H3. *Nat Rev Mol Cell Biol* 13(2):115–126.
27. Rose IA (1980) The isotope trapping method: Desorption rates of productive E.S complexes. *Methods Enzymol* 64:47–59.
28. Westaway KC (2006) Using kinetic isotope effects to determine the structure of the transition states of SN2 reactions. *Advances in Physical Organic Chemistry*, ed Richard JP (Academic, London), Vol 41, pp 217–273.
29. Swain CG, Stivers EC, Reuwer JF, Schaad LJ (1958) Use of hydrogen isotope effects to identify the attacking nucleophile in the enolization of ketones catalyzed by acetic acid 1-3. *J Am Chem Soc* 80(21):5885–5893.
30. Hegazi MF, Borchardt RT, Schowen RL (1979) alpha-Deuterium and carbon-13 isotope effects for methyl transfer catalyzed by catechol *O*-methyltransferase. SN2-like transition state. *J Am Chem Soc* 101(15):4359–4365.
31. Zhang J, Klinman JP (2011) Enzymatic methyl transfer: Role of an active site residue in generating active site compaction that correlates with catalytic efficiency. *J Am Chem Soc* 133(43):17134–17137.
32. Ruggiero GD, Williams IH, Roca M, Moliner V, Tuñón I (2004) QM/MM determination of kinetic isotope effects for COMT-catalyzed methyl transfer does not support compression hypothesis. *J Am Chem Soc* 126(28):8634–8635.
33. Lameira J, Bora RP, Chu ZT, Warshel A (2015) Methyltransferases do not work by compression, cratic, or desolvation effects, but by electrostatic preorganization. *Proteins* 83(2):318–330.
34. Qiao Q, et al. (2011) The structure of NSD1 reveals an autoregulatory mechanism underlying histone H3K36 methylation. *J Biol Chem* 286(10):8361–8368.
35. Couture JF, Collazo E, Hauk G, Trievel RC (2006) Structural basis for the methylation site specificity of SET7/9. *Nat Struct Mol Biol* 13(2):140–146.
36. Couture JF, Dirk LM, Brunzelle JS, Houtz RL, Trievel RC (2008) Structural origins for the product specificity of SET domain protein methyltransferases. *Proc Natl Acad Sci USA* 105(52):20659–20664.
37. Zhang X, et al. (2003) Structural basis for the product specificity of histone lysine methyltransferases. *Mol Cell* 12(1):177–185.
38. Frisch MJ, et al. (2009) *Gaussian 09* (Gaussian, Wallingford, CT).
39. Anisimov V, Paneth P (1999) ISOEFF98. A program for studies of isotope effects using Hessian modifications. *J Math Chem* 26(1-3):75–86.
40. Gonzalez-James OM, et al. (2010) Experimental evidence for heavy-atom tunneling in the ring-opening of cyclopropylcarbinyl radical from intramolecular ^{12}C/^{13}C kinetic isotope effects. *J Am Chem Soc* 132(36):12548–12549.
41. Vetticatt MJ, Singleton DA (2012) Isotope effects and heavy-atom tunneling in the Roush allylboration of aldehydes. *Org Lett* 14(9):2370–2373.
42. Zhang J, Kulik HJ, Martinez TJ, Klinman JP (2015) Mediation of donor–acceptor distance in an enzymatic methyl transfer reaction. *Proc Natl Acad Sci USA* 112(26): 7954–7959.
43. Horowitz S, et al. (2013) Conservation and functional importance of carbon-oxygen hydrogen bonding in AdoMet-dependent methyltransferases. *J Am Chem Soc* 135(41):15536–15548.
44. Horowitz S, Yesselman JD, Al-Hashimi HM, Trievel RC (2011) Direct evidence for methyl group coordination by carbon-oxygen hydrogen bonds in the lysine methyltransferase SET7/9. *J Biol Chem* 286(21):18658–18663.
45. Hu P, Zhang Y (2006) Catalytic mechanism and product specificity of the histone lysine methyltransferase SET7/9: An ab initio QM/MM-FE study with multiple initial structures. *J Am Chem Soc* 128(4):1272–1278.
46. Zhang X, Bruice TC (2007) A quantum mechanics/molecular mechanics study of the catalytic mechanism and product specificity of viral histone lysine methyltransferase. *Biochemistry* 46(34):9743–9751.
47. Zhang X, Bruice TC (2007) Catalytic mechanism and product specificity of rubisco large subunit methyltransferase: QM/MM and MD investigations. *Biochemistry* 46(18): 5505–5514.
48. Zhang X, Bruice TC (2008) Mechanism of product specificity of AdoMet methylation catalyzed by lysine methyltransferases: Transcriptional factor p53 methylation by histone lysine methyltransferase SET7/9. *Biochemistry* 47(9):2743–2748.
49. Zheng W, et al. (2012) Sinefungin derivatives as inhibitors and structure probes of protein lysine methyltransferase SETD2. *J Am Chem Soc* 134(43):18004–18014.
50. Parkin DW, Leung HB, Schramm VL (1984) Synthesis of nucleotides with specific radiolabels in ribose. Primary ^{14}C and secondary ^{3}H kinetic isotope effects on acid-catalyzed glycosidic bond hydrolysis of AMP, dAMP, and inosine. *J Biol Chem* 259(15): 9411–9417.
51. Singh V, Lee JE, Núñez S, Howell PL, Schramm VL (2005) Transition state structure of 5'-methylthioadenosine/S-adenosylhomocysteine nucleosidase from *Escherichia coli* and its similarity to transition state analogues. *Biochemistry* 44(35):11647–11659.
52. Markham GD, Hafner EW, Tabor CW, Tabor H (1980) *S*-Adenosylmethionine synthetase from *Escherichia coli*. *J Biol Chem* 255(19):9082–9092.
53. Jiang Y, et al. (2011) Methyltransferases prefer monomer over core-trimmed nucleosomes as in vitro substrates. *Anal Biochem* 415(1):84–86.
54. Poulin MB, Du Q, Schramm VL (2015) Chemoenzymatic synthesis of ^{36}S isotopologues of methionine and *S*-adenosyl-L-methionine. *J Org Chem* 80(10):5344–5347.
55. Kim S, Bolton EE, Bryant SH (2013) PubChem3D: Conformer ensemble accuracy. *J Cheminform* 5(1):1–17.
56. Forneris F, Binda C, Vanoni MA, Mattevi A, Battaglioli E (2005) Histone demethylation catalysed by LSD1 is a flavin-dependent oxidative process. *FEBS Lett* 579(10): 2203–2207.

BIOCHEMISTRY